ACS APPLIED MATERIALS & INTERFACES

RESEARCH ARTICLE

www.acsami.org

Colloidally Templated Two-Dimensional Conducting Polymer Arrays and SAMs: Binary Composition Patterning and Chemistry

Roderick B. Pernites, Mary Jane L. Felipe, Edward L. Foster, and Rigoberto C. Advincula*

Department of Chemistry and Department of Chemical and Biomolecular Engineering, University of Houston, Houston, Texas, 77204-5003, United States

Supporting Information

ABSTRACT: A facile approach and strategy toward binary-composition, two-dimensional (2D) patterned surfaces of conducting polymer periodic arrays, together with thiol self-assembled monolayers (SAMs) is described. The method involved a Langmuir−Blodgett (LB)-like deposition of latex microsphere particles, electropolymerization via cyclic voltammetric (CV) techniques, and self-assembly of an amphiphile. The LB-like technique enabled the monolayer deposition of different sizes of polystyrene (PS) particles in hexagonal packing arrangement on planar substrates. Combining the LB-like method with CV electropolymerization is advantageous because it provides deposition control of a polymer interconnected network, controlled composition ratio of polymer and SAMs, and control of 2D size and spacing of the spherical void pattern. Electrochemical-quartz crystal microbalance (EC-QCM) in situ monitoring of the film deposition quantified a constant and linear growth rate, with varying viscoelastic behavior of the conducting polymer adsorption on planar and PS-templated substrates. The dual-patterned surface provided a good imaging contrast as observed by atomic force microscopy (AFM). Complementary analyses such as X-ray photoelectron spectroscopy (XPS), attenuated total internal reflection infrared (ATR IR) spectroscopy, ultraviolet-visible (UV−vis) spectroscopy, and static contact angle measurements were used to characterize the formation of the patterned surface. The versatility of the method enables the potential for making various types of quantitative binary compositions and patterned surfaces using different combinations of conducting polymer or functional SAMs, which can be extended in the future to polymer brushes and layer-by-layer assembly of various materials.

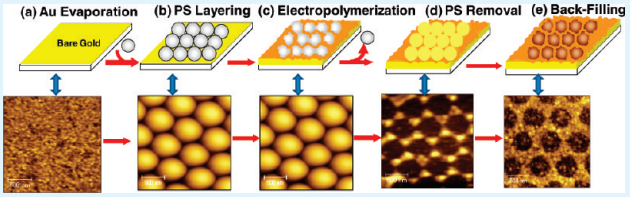

KEYWORDS: electropolymerization, colloidal particles, conducting polymer, self-assembly

1. INTRODUCTION

Recently, there has been significant interest in the assembly of ordered colloidal crystals (called synthetic opals) that serve as sacrificial templates for structuring macroporous inverse colloidal crystals (called inverse opals or triangular arrays) with potential applications ranging from photonic crystals to bioreactors.[1−7] Examples of sacrificial templates include anodized alumina,[8−10] diblock copolymers,[11−14] and organic or inorganic colloidal crystals.[15−17] Among them, colloidal crystals stand out to be the most eminent, because they are robust and easy to handle. Inverse opals are manufactured from scores of materials such as metals,[18,19] inorganic oxides,[15−17] diamond and glassy carbon,[20] or conducting polymers.[21−29] The latter one is the most appealing and promising, because they can be easily processed with the feasibility of tuning their physicochemical properties. More importantly, conducting polymers are known to have unique and interesting electrical,[30,31] electronic,[32−34] and optical[35] properties that can be modified by design and synthesis.[36] However, not many have been focused on using them for templating or micropatterning "2-D chemistry" on various surfaces, despite the myriad applications of micropatterned surface on semiconductors, microelectromechanical systems (MEMS), biochips, biosensors, cell-growth regulation, micro/nanofluidic systems, etc.[37−41] To date, patterned surfaces are normally produced by toilful and sophisticated lithographic techniques[42] such as soft-lithographic microcontact printing,[43,44] UV/electron-beam lithography,[45] scanning probe lithography,[46] and imprint lithography.[47] Herein, we report the formation of highly ordered 2D monolayer arrays with a binary composition of conducting polymer pores and triangular arrays or objects along with self-assembled monolayers (SAMs) of an organo-thiol. This was accomplished by using a rapid and inexpensive approach with no requirement of intricate instrumental setup. To the best of our knowledge, no report has been made about the fabrication of dual-patterned inverse colloidal crystals that combines a conducting polymer and a monolayer alkanethiol self-assembly in a 2D manner. Most, if not all, polymeric inverse opals are multilayer and hierarchical, which is not ideal for binary component patterning.

In this study, the fabrication scheme combined the LB-like technique[48] and an electropolymerization process called colloidal template-assisted electropolymerization or template-directed

Received: November 26, 2010
Accepted: February 10, 2011
Published: February 28, 2011

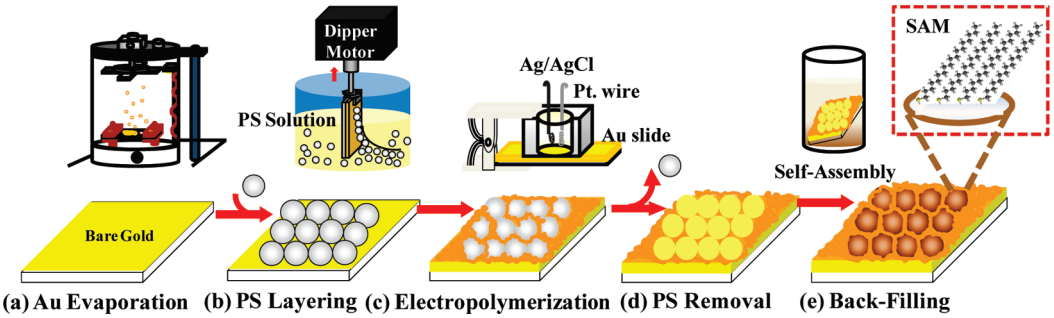

Figure 1. Fabrication of highly ordered monolayer colloidal crystals and inverse patterned colloidal crystals of conducting polymer film.

electrosynthesis, followed by polystyrene (PS) particle removal (see Figure 1). The process was done under ambient conditions pivotal to further surface alteration of the unmodified areas, including layer-by-layer assembly, SAM, growth of polymer brush, and another electrodeposition. However, in this study, the modification of the unpatterned surface is first demonstrated using SAM immobilization of 1-octadecanethiol (1-ODT) as a model organo-thiol. Until now, colloidal template 2D electropolymerization remains largely an unexplored method, and there are only a few accounts on colloidal template electropolymerization technique for micropatterning polymer films, which were published by Yanagida,[22] Bartlett,[23,24] Caruso,[5,25,26] and Knoll.[28] In addition, the same technique was also used for making highly ordered macroporous structures via the electrodeposition of metals (e.g., gold, platimum, nickel, palladium, and cobalt)[49−53] and metal oxides (e.g., iridium oxide, zinc oxide)[54,55] between the void spaces of the sacrificial template colloidal particles.

As shown in Figure 1b, the colloidal crystals were formed using the LB-like technique that provides a single layer of highly ordered deposition of latex submicrospheres on a flat substrate surface at the air/liquid interface via the vertical lifting technique.[48] The colloidal pattern then becomes a mask for the in situ electropolymerization of electro-active monomers in making an inverse opal. For this study, a bis-carbazole monomer (CBz TEG G1) with pregrafted ethylene glycol units was used for electropolymerization (see the synthesis described in Scheme 1). The proposed method is facile because of (1) control of the deposition of the polymer film by various electrochemical process parameters (e.g., current, scan rate, potential window, etc.) and (2) control of the 2D size of the arrays by simply changing the size of the colloidal sphere masks. The proposed method promises to be versatile, because the periodic pattern can be fabricated on various conducting electrode substrates including gold, indium tin oxide (ITO), stainless steel, alumina, etc. electrodes via electropolymerization. Our group has demonstrated the electrodeposition of conducting and conjugated polymer network (CPN) polymers onto different electrode substrates such as ITO,[56,57] steel,[58] and Au-coated glass or Au-coated silicon wafer.[59−61] Furthermore, a repertoire of different types of conducting polymers (polythiophene, polypyrrole, polyaniline, etc.) is readily and commercially available for electropolymerization. In principle, the potential of this technique is in incorporating specific compositions of redox active and electrically conducting polymers within a periodic vicinity of surface attached molecular and macromolecular moieties (e.g., surfactants, tethered polymers, biomolecules). This, in turn, will enable a more effective and specific field effect or stimuli response for these molecules mediated by the presence of the conducting polymer. The patterning then becomes a method for composition control rather than the object of primary interest for image resolution or design, although both functions can be combined.

2. RESULTS AND DISCUSSION

Figure 2 presents the AFM 2D topographic images with 3D images on inset for the 200-nm (Figure 2a), 350-nm (Figure 2b), and 500-nm (Figure 2c) PS particle layers on a Au substrate. The layering of 500-nm-sized PS was also accomplished on an ITO substrate (Figure 2d) to assess the feasibility of the method on other conducting substrates with different surface roughness. A well-ordered and closely packed single-layer assembly of the colloidal crystals in hexagonal packing arrangement is clearly seen on Au substrates (root-mean-square (rms) roughness of 0.77 ± 0.05 nm) and ITO substrates (rms of 2.00 ± 0.19 nm). The monolayer ordering of the microsphere particles has been reported to be dependent on parameters of the LB-like technique and the concentration of the particles and surfactant (in this case, sodium *n*-dodecyl sulfate (or SDS)) in solution.[48] The same AFM images are also observed even after the electropolymerization of the functional and cross-linking monomer (CBz TEG G1) onto the PS layer on the Au electrode substrate, indicating that the electrodeposition of the conducting polymer is limited within the interstitial voids spaces between the PS particles. It is worth mentioning that the original high ordering in hexagonal assembly of the latex spheres on the surface is not disrupted by the electropolymerization process under the current conditions (see Figure S1 in the Supporting Information). This result is made possible by using the correct solvent, such as acetonitrile, during electropolymerization. The electropolymerization of the monomer was accomplished by using the CV technique, in which the optimized parameter entails the sweeping of the potential from 0 V to 1.1 V at 50 mV/s for 20 cycles.

The layering of the PS particles was also achieved on Au-QCM crystal such that the electrodeposition of the conducting polymer can be monitored in situ by electrochemistry EC-QCM measurements (see Figure 3). To our knowledge, this is the first study on the use of EC-QCM to monitor the electrodeposition of a conducting polymer onto a colloidal templated Au-QCM crystal and also the first report on the use of carbazole toward the formation of 2D patterned surface via colloidal template electropolymerization. This hyphenated technique (EC-QCM) was used extensively by our group to study the in situ formation of conducting polymer films.[62−64] The cyclic potential growth of the polymer film on bare Au-QCM crystal is shown in Figure 3a. In the first anodic scan (the first CV cycle), the oxidation peak with an onset potential at ~1.0 V is attributed to the formation of

Scheme 1. Synthesis of the Functional and Cross-Linking Monomer (CBz TEG G1)

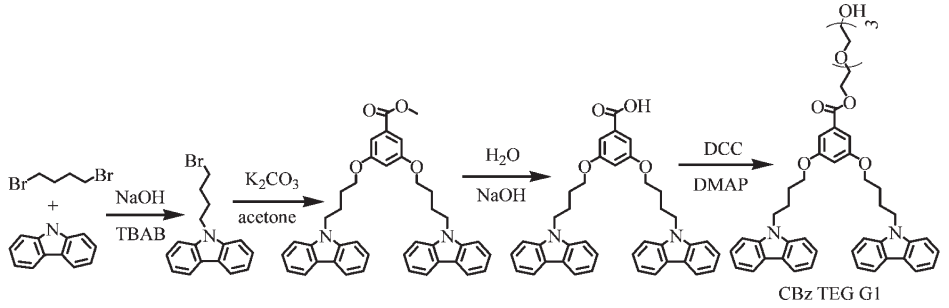

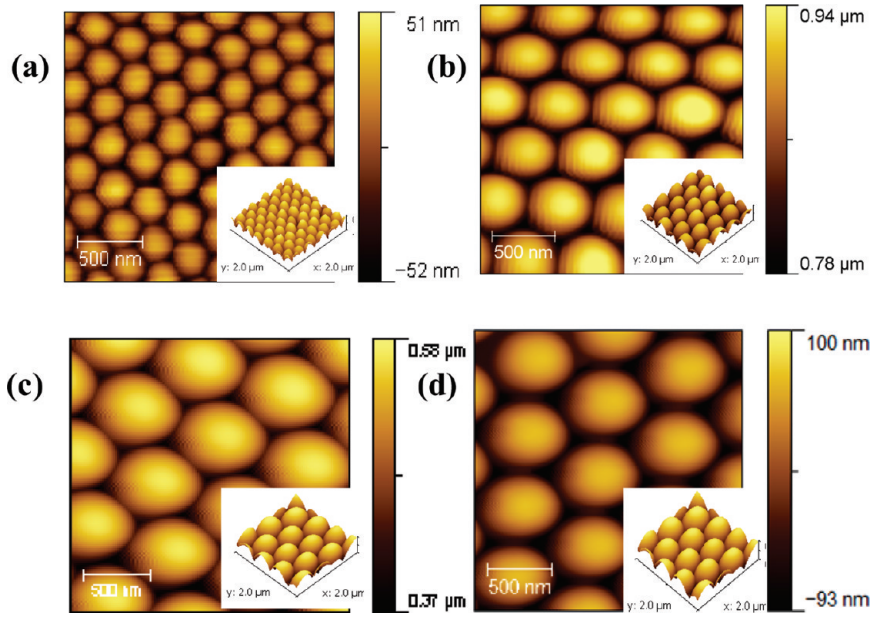

Figure 2. AFM topography 2D images (3D on inset) of the different sizes of PS assembled on Au ((a) 200 nm, (b) 350 nm, and (c) 500 nm) and (d) 500 nm PS assembled on ITO.

a radical cation (called a polaron) from the removal of an electron in the nitrogen atom of the N-substituted carbazole monomer.[65,66] The carbazole has been reported to be oxidized electrochemically beyond +1.0 V.[65] Upon reduction (cathodic scan), this reactive radical cation readily combines with another radical cation or with a parent molecule to form two types of dicarbazyls with the 3,3′-bicarbazyl as the predominant product.[65] In the second cycle, a new oxidation peak appears (between 0.7 V and 0.9 V) at a relatively lower potential, with a corresponding reduction peak in the reverse scan, from 0.68 V to 0.88 V. This new anodic peak is related to the formation of a more-stable dication (bipolaron) with extendend π-conjugation, because of the oxidation of the 3,3′-bicarbazyl,[67,68] which is oxidized easier than carbazole.[65] Upon succeeding CV cycles until the 20th cycle, the current increases at this reduction−oxidation (redox) peak, indicating the formation of more conjugated species as a result of further cross-linking between the carbazole units and electrodeposition of the material onto the Au electrode substrate.[69] Concurrently, the higher anodic peak (with the onset potential at ∼1.0 V) that is ascribed to the oxidation of the carbazole monomer[65] decreases slightly from the 1st CV cycle to the 20th CV cycle. This result is realistic because the monomer in solution is being depleted during the course of the electrochemical polymerization. The presence of electrodeposited material was confirmed by performing a monomer free scan (see the inset in Figure 3a), sweeping the potential on the same voltage window as the electropolymerization, but for one CV cycle in the solvent (acetonitrile) with the supporting electrolyte (0.1 M TBAH) only. Note that this CV scan was done after electropolymerization and thorough rinsing of the film with the solvent to remove any excess monomers. The appearance of an identical CV curve with the same reduction−oxidation (redox) peaks corroborated the successful and well-behaved electrodeposition of the conducting polymer. The current increase in the redox peak during electropolymerization is accompanied by a change in frequency of the quartz crystal. Figure 3b depicts a recurring oscillation in the ΔF change of the QCM crystal for each CV cycle as the polymer film switches from oxidized to reduced states.[70] Upon oxidation of the polymer (doping process), the ΔF value decreases and then slightly increases upon reduction and eventually stabilizes at a neutral state (0 V). During doping,[70−72] the poly(carbazole) becomes

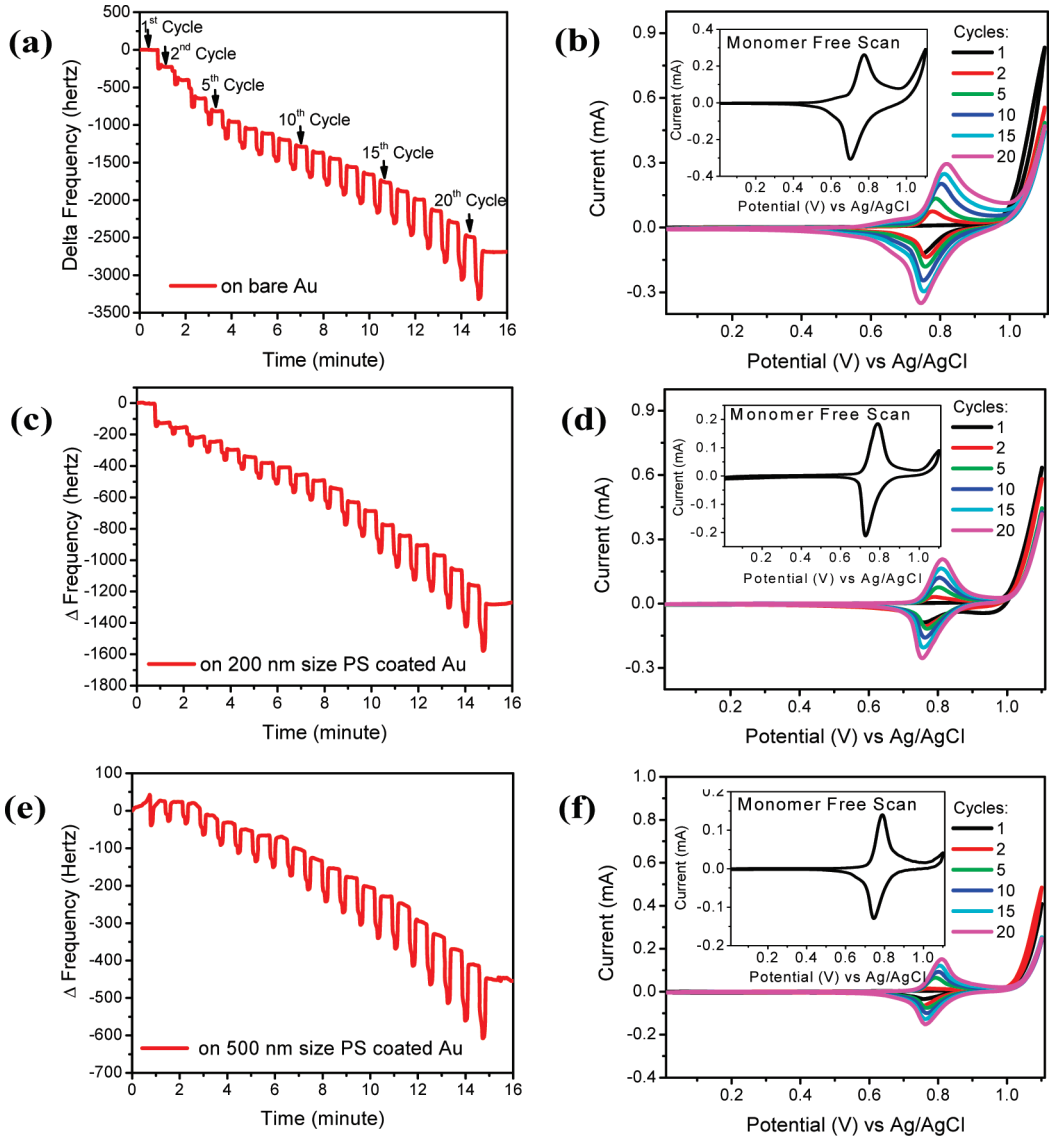

Figure 3. In situ EC-QCM measurements of the electrodeposition of CBz TEG G1 on (a, b) bare Au, (c, d) 200-nm PS layered Au, and (e, f) 500-nm PS layered Au. Note that panels a, c, and e depict the QCM responses and panels b, d, and f show the CV diagrams with post-polymerization scan insets called "monomer free scans".

positively charged and, thus, accepts/adsorbs a counterion (in this case, PF_6^- from the TBAH supporting electrolyte) from solution causing the ΔF value to decrease. Upon dedoping (0 V),[70−72] the polymer film returns to its neutral state and, hence, ejects the counterion back to the bulk solution. This makes the ΔF value slightly increase and then plateau. The overall deposition of the poly(carbazole) on Au-QCM crystal is evidenced by the net decrease in the ΔF value after 20 CV cycles. Notice that the QCM response exhibits a linear ($R > 0.99$) and constant step decrease in the ΔF value, which corresponds with the linear ($R > 0.98$) increase of current in the redox peak during electropolymerization (see the linear fitting of data points in Figure S2 in the Supporting Information), signifying a well-behaved and linear growth rate film formation. The trace of the CV diagram, the position of the redox couple, and the oscillating EC-QCM response are similar to that observed with the 200-nm PS layered substrates (Figures 3c and 3d) and the 500-nm PS layered substrates (Figures 3e and 3f). However, the electropolymerization of the monomer directly on planar Au has shown a higher ΔF change in solution (−2676.34 Hz ± 14.39) than with the 200-nm PS-coated Au-QCM crystal (−1274.78 Hz ± 8.18) and the 500-nm PS-coated Au-QCM crystal (−447.31 Hz ± 4.79), indicating that more material has been deposited on bare Au. The same order is kept in the QCM measurement in air after removing the solution and drying the crystal completely. By using the simplified Sauerbrey equation (eq 2 in the Supporting Information), the average mass adsorbed due to the electrodeposited film is determined as follows: 66.57 μg (onto planar Au), 22.19 μg (onto 200 nm PS-coated Au), and 8.97 μg (onto 500 nm PS-coated Au). A similar trend is observed in the CV diagram, which shows a higher redox current in the electropolymerization of the monomer on bare Au-QCM crystal than with the 200-nm PS-coated Au-QCM crystal (Figure 3d) and the 500-nm PS-coated Au-QCM crystal (Figure 3f). These results were anticipated, since the PS layer serves as a potential barrier to the electrodeposition of the film, limiting access only

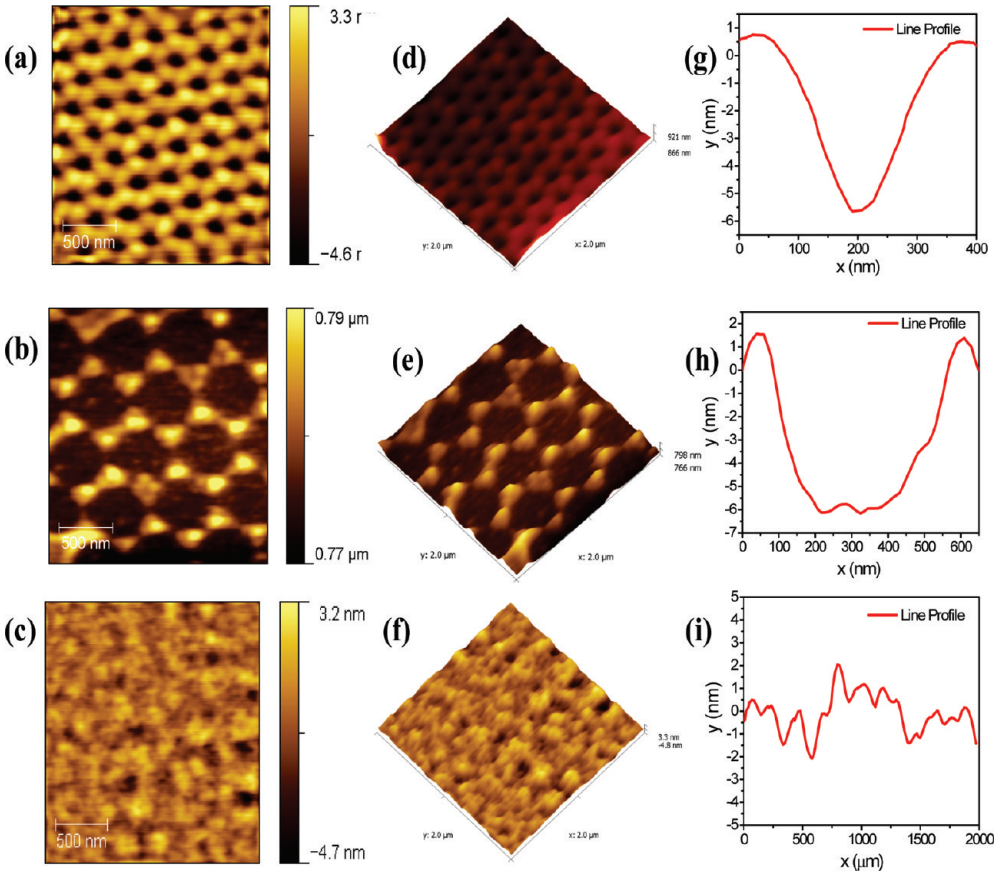

Figure 4. AFM topography (2D and 3D) images of poly(CBz TEG G1) on (a, d) a 200-nm PS-templated substrate, (b, e) a 500-nm PS-templated substrate, and (c, f) bare Au. AFM line profile analyses of poly(CBz TEG G1) on 200-nm and 500-nm PS-templated substrates and bare Au ((g) 200-nm PS-templated substrate, (h) 500-nm PS-templated substrate, and (i) bare Au) are also shown.

through the interstitial voids. Similarly, the same redox couple due to poly(carbazole) is seen in the monomer free scan for the electrodeposition of the conducting polymer onto the 200-nm PS-coated substrate (Figure 3d inset) and the 500-nm PS-coated substrate (Figure 3f). Futhermore, a plot of ΔF versus ΔR (defined as motional resistance) is obtained to determine the changes in viscoelastic behavior of the film during electropolymerization (see Figure S3 in the Supporting Information). A larger change implies a more viscoelastic behavior of the film.[63,73] The electrodeposition on bare Au displays a relatively smaller and regular change in the ΔR vs ΔF relationship than that on PS-templated substrates, indicating a more rigid film deposition on Au.[63,73]

After electrodeposition, the PS particle sacrificial templates are then washed with THF to reveal the underlying electrodeposited materials. Note that DCM and toluene can also be used in removing the PS particle from the surface. The AFM 2D images (Figures 4a and 4d) and 3D images (Figures 4b and 4e) present a well-ordered monolayer array of conducting polymer pores (from 200 nm) and triangular objects (from 500 nm) or simply inverse colloidal monolayer arrays, respectively. A thicker cavity wall is observed with the smaller 200-nm template particle size (see Figures 4a and 4d). This outcome supports the earlier QCM data that more material has been adsorbed with the electropolymerization onto 200-nm PS-coated Au-QCM crystal than onto 500-nm PS-coated Au-QCM crystal. For both sizes, a uniform pore cavity diameter is observed with the PS-templated surfaces.

The conducting polymer adsorbed on bare Au was also scanned in the AFM (see Figures 4c and 4f), which shows a homogeneous film and a different surface morphology than that of bare Au (see Figure S4 in the Supporting Information). For instance, the fine grains or globular-shaped domains, which are typical for a bare Au surface, are no longer visible in the topography image (see Figure 4c) after the electrodeposition of the poly(carbazole), suggesting complete coverage. Moreover, the AFM line profile has changed, deviating from a narrow and more regular increase and decrease in the x-axis ($\pm$ 1 nm) (compare Figure 4i with Figure S4b in the Supporting Information). This result is coherent with our recent report[74] about the change in the surface morphology of the pristine Au substrate after the electropolymerization of a carbazole monomer with a pregrafted reversible addition−fragmentation chain transfer (RAFT) agent. The thickness of the poly(carbazole) film electrodeposited on bare Au was determined by ellipsometry to be 27.96 $\pm$ 1.35 nm. The AFM cross-sectional analyses of the 200-nm PS-templated polymer film (Figure 4g) and the 500-nm PS-templated polymer film (Figure 4h) show high regularity in the line profile, with an estimated height of wall cavity or peak-to-baseline distance of 6.52 $\pm$ 0.56 nm and 8.18 $\pm$ 1.04 nm, respectively (see Figures S5 and S6 in the Supporting Information). In contrast, a random profile is shown with the electropolymerization onto the planar Au (Figure 4i). Furthermore, a scanning electron microscopy (SEM) image reveals high periodicity of the 500-nm size PS-imprinted polymer film with an

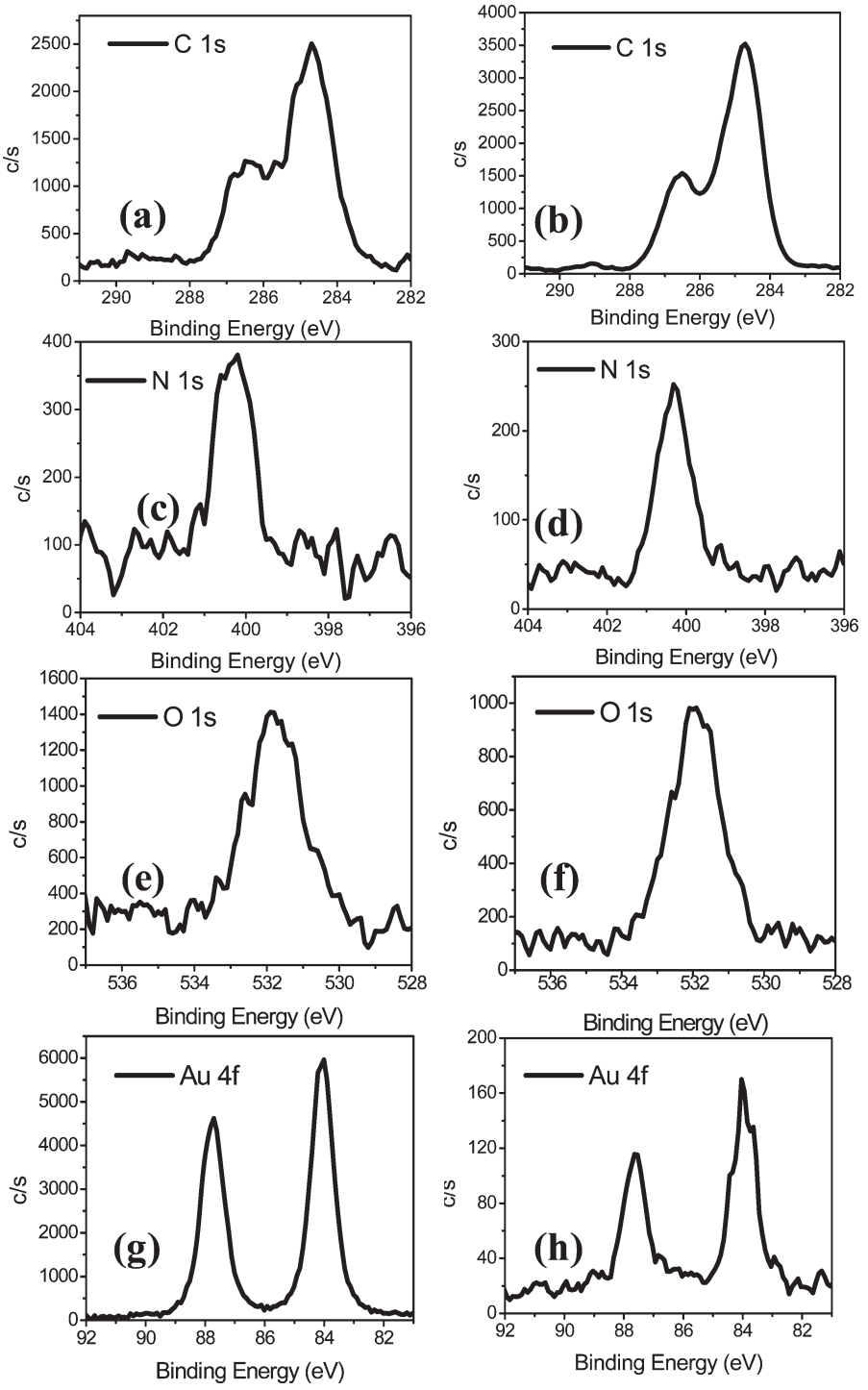

Figure 5. X-ray photoelectron spectroscopy (XPS) high-resolution scans of the 500-nm PS-templated poly(CBz TEG G1) on Au (after the removal of 500-nm size PS) (left column) and poly(CBz TEG G1) on bare Au (right column): (a, b) C 1s; (c, d) N 1s; (e, f) O 1s; and (g, h) Au 4f.

exact size of the cavity equivalent to 500 nm, as determined from the SEM cross-sectional analysis (see Figure S7 in the Supporting Information).

To further validate the formation of the poly(carbazole), complementary XPS measurements were carried out with the electropolymerized films. The high-resolution XPS scans (Figures 5a−f) present the expected elements due to the conducting polymer film, such as carbon (283−290 eV), nitrogen (398−402 eV), and oxygen (529−534 eV), which are consistent with the published literature.[75,76] The C 1s peak (Figures 5a and 5b) with the highest intensity located at ∼284.7 eV is assigned to the C−C and C−H moieties, while the small shouldering peaks at ∼285.4 eV and ∼286.6 eV are attributed to the C−N and C−O moieties, respectively.[75] The almost negligible peak at ∼288.9 eV in the C 1s spectrum is ascribed to the O−C═O functional group,[74,77] which is the least-abundant functional group in the structure. The symmetrical N 1s peak (Figures 5c and 5d) centered at ∼400.3 eV is assigned to

Table 1. XPS Elemental Composition Analysis of the Electropolymerized CBz TEG G1

substrate		Elemental Composition (%)		
		C	N	O
	theoretical value	78.33	3.88	17.77
on bare Au	experimental result	80.55	3.38	16.07
on 500-nm PS-coated Au (after PS removal)	experimental result	78.53	4.03	17.45

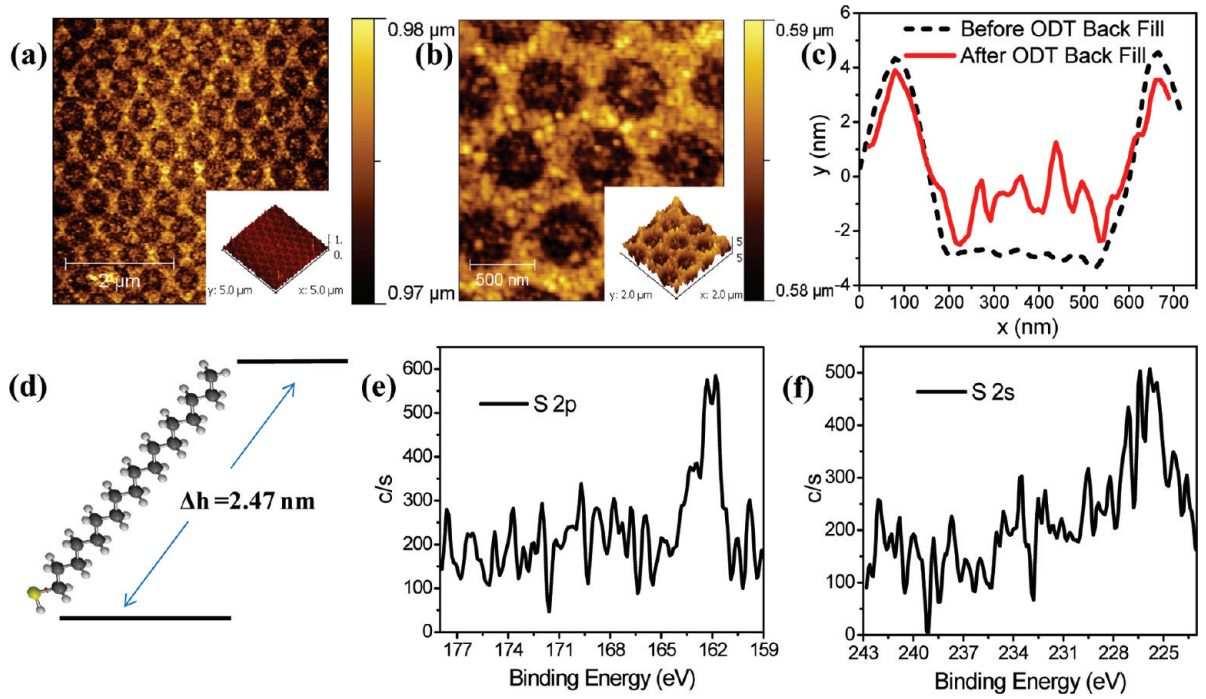

Figure 6. AFM topography images (3D on inset) of a 500-nm backfilled templated array ((a) 5 μm × 5 μm and (b) 2 μm × 2 μm scans), along with (c) line profile analysis before and after backfilling with 1-ODT. (d) Structure and theoretical length of 1-ODT, as calculated by Spartan wave function software. XPS high-resolution scans of (e) S 2p and (f) S 2s peaks after backfilling of the inverse colloidal crystal.

the nitrogen element of the carbazole ring.[78] The O 1s spectrum (Figures 5e and 5f) shows maximum peak intensity at 531.9 eV and a shouldering peak at 530.5 eV, which are assigned to the C—O and C═O moieties, respectively.[75] The Au 4f peak (Figures 5g and 5h) that displays a doublet peak ($4f_{7/2}$ and $4f_{5/2}$) with a separation distance of ~3.6 eV is due to the metallic Au substrate.[79] It has a greater peak area and intensity in the 500-nm PS-templated substrate than in the electropolymerized film on bare Au (compare Figure 5g to Figure 5h). There is a decrease in the peak area of the Au 4f by more than 95% with the electropolymerized film on Au. This finding is expected because (1) a more porous film is created with the PS-templated substrate, which exposes some area of the Au surface after PS removal, and (2) a thicker polymer film is formed with electropolymerization directly on bare Au, as determined by the earlier EC-QCM and thickness measurements. The relative atomic concentrations (summarized in Table 1) for the electrodeposition of the conducting polymer onto the 500-nm PS-coated Au are in close agreement with the expected atomic percentage (given in parentheses): C, 78.53% (78.33%); N, 4.03% (3.88%); and O, 17.45% (17.77%). Aside from the Au peak due to the substrate, these are the only elements present in the wide scan, implying a clean polymer surface (see Figure S8 in the Supporting Information). A similar result is determined with the electropolymerization on bare Au (Table 1). The results of the XPS measurements were also validated by ATR IR (see Figure S9 in the Supporting Information) and UV—vis (see Figure S10 in the Supporting Information) analyses, which showed the signature peaks of the electrodeposited conducting polymer.

To demonstrate dual chemistry on the highly ordered array surface, the experiment was continued by backfilling the cavities of the 500-nm PS-templated polymer film with 1-ODT SAM. Through this extension, a highly ordered array of a conducting polymer material was proven to coexist on a surface with an organic monolayer film through thiol assembly (i.e., inside the pores). It also follows that other thiols or another conducting polymer can be used for backfilling purposes. In fact, the availability of the unmodified Au surface should make it amenable for other Au surface chemistries, including metal deposition and polymer brush synthesis. The change in the surface morphology of the AFM images in Figures 6a and 6b confirms the backfilling of the cavities with the 1-ODT SAM. Moreover, the rms value of the inside pore surface increases from 0.80 ± 0.12 nm to 1.20 ± 0.10 nm after 1-ODT adsorption. As a control, the rms value of the bare Au slide (0.77 ± 0.05 nm; see Figure S4a in the Supporting Information) was also measured prior to

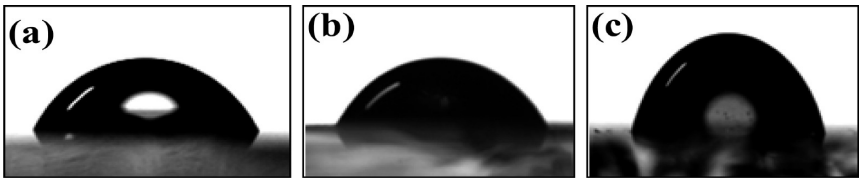

Figure 7. Static water contact angle measurements of (a) poly(CBz TEG G1) on bare Au, (b) 500-nm PS-templated poly(CBz TEG G1), and (c) 1-ODT backfilled PS-templated poly(CBz TEG G1).

surface modification, which is close to the rms of the inside pores before 1-ODT immobilization. As seen from the AFM images, the 1-ODT is adsorbed all the way to the cavity walls of the conducting polymer array, which also created a better contrast, transforming the prism-like features to more of a highly regular network structure. A similar dual-patterned surface with a high degree of ordering is possible, as reported by Liu et al.,[80] but requires a more sophisticated and tedious fabrication procedure. Also, from the line profile (Figure 6c), the cavities are clearly shown to be filled with the 1-ODT, as evidenced by the increase in height and uneven line profile of the holes and the decrease in peak-to-baseline distance. From molecular mechanics (Spartan '08 (v1.2.0) calculations, the theoretical length of the fully extended 1-ODT was calculated to be ~2.47 nm (see Figure 6d). This value is close to the difference in length of the peak-to-baseline before and after the backfilling step with 1-ODT at ~2.36 nm (compare Figure S6 and S11 in the Supporting Information). Moreover, the appearance of sulfur (S 2p and S 2s peaks) in the XPS high-resolution scans (see Figures 6e and 6f), which can *only* be due to the elemental sulfur of the thiol end group, strongly confirms the chemisorption of 1-ODT.[81] Because of spin−orbit splitting,[82,83] the S 2p peak (Figure 3e) is a known doublet (2:1 intensity ratio) assigned as $2p_{3/2}$ (~162.0 eV) and $2p_{1/2}$ (~163.3 eV), and the sulfur peak at this range corresponds to the bound sulfur.[81,83]

Static contact angle measurements in water were also carried out with the electropolymerized arrays to confirm changes in surface energy. The electrodeposited CBz TEG G1 on planar Au gave an angle of 56° ± 1° (Figure 7a), which is higher than that for the 500-nm size PS-coated Au (46° ± 1°) before electropolymerization. The inverse colloidal crystals of the electropolymerized CBz TEG G1 on Au showed a contact angle value of 58° ± 2° (Figure 7b), which is closer to the electropolymerized film on bare Au. The backfilling of 1-ODT onto the cavities of the PS imprinted polymer film resulted in ~12° increase in water contact angle of the film (70° ± 1°) (Figure 7c), approaching the contact angle of the 1-ODT assembled on bare Au. Its measured value is equivalent to 103° ± 1°. Therefore, the increase in the hydrophobicity of the dual-patterned surface is attributed to the backfilling of the holes with the hydrophobic molecule 1-ODT.

3. CONCLUSION

In conclusion, we have demonstrated a facile approach to a binary compostion of highly ordered 2-D conducting polymer pores and/or array objects by template-directed electropolymerization with SAM patterning in thin films. This work illustrates the generalization of a colloidal template methodology for the production of high-surface-area monolayer nano/macroporous structures of polymer objects. The polymer network electrosynthesis displayed a smooth CV deposition, as observed by EC-QCM and verified using AFM, XPS, and contact angle measurements. The backfilling of the inside cavities by the SAM approach resulted in a "2-D binary patterned chemistry". Thus, this procedure provides an alternative route toward the fabrication of dual-patterned surfaces, which are usually accomplished by more complicated and more expensive lithographic and nonlithographic methods. Because of the versatility of the fabrication scheme, the holes also can be used for other electropolymerization and electrografting[74,84] procedures. Several patterning protocols combining the deposition of polymer brushes via surface-initiated polymerization (SIP) and the use of molecularly imprinted polymers (MIPs) are being pursued by our group.

4. EXPERIMENTAL SECTION

4.1. Materials. The polystyrene (PS) latex microbeads (200- and 500-nm sizes, 2.5 wt % solids in aqueous suspension) were purchased from Polysciences, Inc. and used without further purification. Acetonitrile (ACN), sodium *n*-dodecyl sulfate (SDS), 1-octadecanethiol (1-ODT), tetrahydrofuran (THF), and tetrabutylammonium hexafluorophosphate (TBAH) were obtained from Sigma−Aldrich. The glass slides (BK 7) were acquired from VWR Scientific Products. The monomer (carbazole (CBz) of generation 1 (G1) with pregrafted tetraethylene glycol unit (TEG) (or abbreviated as CBz TEG G1) used in electropolymerization was synthesized in our laboratory, and the details of the synthesis are reported in the Scheme S1 in the Supporting Information. The deionized water (18.2 MΩ cm) used for the dilution of PS particles was purified by a Milli-Q Academic system (Millipore Corporation) with a 0.22-μm Millistack filter at the outlet. The PS solution used for layering contained 1 wt % PS particles and 34.7 mM SDS (spreading agent) in Milli-Q water. Prior to PS layering on Au-coated BK 7 glass or Au-QCM crystal, the solution was sonicated for ~15−20 min. The solution for electropolymerization was composed of 5 mM CBz TEG G1 (monomer) with 0.1 M TBAH as the supporting electrolyte in ACN. In our previous studies, the monomers of carbazole and terthiophene derivatives were prepared in dichloromethane (DCM). However, in this study, DCM was not used as solvent, because it will remove the layer of PS on the Au substrate.

4.2. Film Preparation. *4.2.1. Gold Deposition.* The Au surface was prepared by thermally evaporating Au (50−100 nm thick) onto the BK 7 glass slide with chromium (Cr) adhesion layer (2−5 nm thick) under high vacuum with a base pressure of 10^{-6} bar (see Figure 1a). The Cr and Au deposition were done at a rate of ~0.4 Å s^{-1} and ~1.1 Å s^{-1}, respectively, using a thermal evaporator (Edwards, Model E-306). The Au surface was subjected to oxygen plasma cleaning (Plasmod, March Instruments) for 120 s before PS deposition.

4.2.2. PS Particle Layering. The layering of PS microbeads was accomplished using a similar procedure described earlier by Grady and co-workers.[48] The method was called the LB-like technique because it formed a monolayer of PS particles onto flat surfaces without using the conventional LB setup that employs floating barriers. As shown in Figure 1b, the substrate was attached into the dipper motor via a Teflon

clip and was dipped into an aqueous solution containing PS particles (1 wt %) and SDS (34.7 mM) as a spreading agent. The substrate then was withdrawn vertically from the solution at a lift-up rate of 0.1−0.3 mm/min. Finally, the substrate was dried by suspending it in air for a few minutes.

4.2.3. Electropolymerization. The electropolymerization of the monomer (Figure 1c) was done using cyclic voltammetric (CV) technique using an Autolab PGSTAT 12 potentiostat (MetrOhm) in a standard three-electrode measuring cell (a fabricated electrochemical cell with a diameter of 1.0 and volume of 0.785 cm^3, Teflon made) with platinum wire as the counter electrode, Ag/AgCl wire as the reference electrode, and the bare Au or PS-coated Au substrate as the working electrode (see Figure 1). The potential was scanned over a range of 0−1.1 V at 50 mV/s for 20 CV cycles. After the electrodeposition, the resulting film was washed with ACN thrice, and a monomer free scan was performed, using exactly the same experimental parameters but for only one CV cycle. The electropolymerized substrate was dried with nitrogen gas. The electropolymerization was also performed on Au-coated QCM crystal or PS layer Au-coated QCM crystal using the above-mentioned conditions and procedures. In this study, a bis-carbazole monomer (CBz TEG G1) with pregrafted ethylene glycol (EG) units was used for the electropolymerization (see the synthesis in Scheme 1). Surfaces modified with EGs have been known to resist the nonspecific adsorption of proteins,[84] and, therefore, find potential applications as biomedical coatings. With a patterned polymer film array using CBz TEG G1, proteins can be possibly adsorbed selectively onto the unmodified surface.

4.2.4. PS Particle Removal. The PS microspheres were removed from the surface after electropolymerization by dipping the PS-coated substrate in THF twice for 30 min. This is done to create the inverse colloidal crystals of conducting polymer pores and arrays (also called inverse opals or PS-templated film). The substrate then was allowed to dry naturally under ambient conditions.

4.2.5. Backfilling of PS Cavities. The PS-imprinted electropolymerized film was dipped into a solution of 1 mM 1-ODT in ethanol for ∼19 h to create a dual-patterned surface of inverse colloidal crystals of conducting polymers with thiol assembly primarily adsorbed onto the macropores. The substrate was rinsed with ethanol for ∼30 min to remove the noncovalently bound thiol molecules. Finally, the substrate was dried with nitrogen gas.

4.3. Instrumentation. *4.3.1. Electrochemistry.* Cyclic voltammetry was performed in a conventional three-electrode cell, using an Autolab PGSTAT 12 potentiostat (Brinkmann Instruments (now MetroOhm USA)). The potentiostat was controlled using GPES software (version 4.9).

4.3.2. Quartz Crystal Microbalance (QCM). The QCM apparatus, probe, and crystals were made available from Maxtek, Inc. AT-cut polished QCM crystal (5 MHz) 13 mm in diameter was used as the working electrode. The data acquisition was done with an R-QCM system that was equipped with a built-in phase lock oscillator and the R-QCM Data-Log software.

4.3.3. Ellipsometry Measurement. The thickness of the electropolymerized film was measured by null ellipsometry, using the Multiskop ellipsometer (Optrel GmbH, Germany) equipped with a 632.8-nm laser. The measurement was done at a 60° angle of incidence under dry and ambient conditions. At least three measurements were performed at various spots of the film. The measured values of Δ and Ψ are used to simulate the thickness of the film, using integrated specialized software (Elli, Optrel) that was provided with the instrument. The refractive index used to calculate the thickness of the unpatterned polymer film is 1.6.[74]

4.3.4. Contact Angle Measurement. A static contact angle analysis of the electropolymerized film was done using a CAM 200 optical contact angle meter (KSV Instruments, Ltd.) with CAM 200 software. The measurement was achieved by making an ∼1 μL drop of Milli-Q water onto the film. At least three measurements were performed at various positions of the film.

4.3.5. Atomic Force Microscopy (AFM) Measurement. The AFM measurements were carried out in a piezo scanner from Agilent Technologies. The scanning rate was set between 0.8 to 1.0 lines/s. Commercially available tapping mode tips (TAP300, Silicon AFM Probes, Ted Pella, Inc.) were used on cantilevers with a resonance frequency in the range of 290−410 kHz. The scanning of the electropolymerized film was performed under ambient and dry conditions. All AFM topographic images (AAC tapping mode) were filtered and analyzed using SPIP (Scanning Probe Image Processor, Imagemet.com) or Gwyddion 2.19 software.

4.3.6. X-ray photoelectron spectroscopy (XPS) measurement. A PHI 5700 X-ray photoelectron spectrometer was equipped with a monochromatic Al Kα X-ray source ($h\nu$ = 1486.7 eV) incident at 90°, relative to the axis of a hemispherical energy analyzer. The spectrometer was operated both at high and low resolutions with pass energies of 23.5 and 187.85 eV, respectively, a photoelectron take off angle of 45° from the surface, and an analyzer spot diameter of 1.1 mm. All spectra were collected at room temperature with a base pressure of 1×10^{-8} Torr. The peaks were analyzed first by background subtraction, using the Shirley routine. All the samples were completely dried in argon gas prior to XPS measurements.

4.3.7. Scanning Electron Microscopy. The morphology of the samples were examined by field-emission scanning electron microscopy (FE-SEM) using a JEOL Model JSM 6330F instrument operating at 15 kV. Prior to SEM analysis, the films were thoroughly dried under vacuum for at least 24 h. SEM images were processed and analyzed using ImageJ software.

■ ASSOCIATED CONTENT

Supporting Information. Detailed information about the experimental procedures and additional experimental data. The material is available free of charge via the Internet at http://pubs.acs.org.

■ AUTHOR INFORMATION

Corresponding Author
*Phone: +1 713 743 1755. E-mail: radvincula@uh.edu.

■ ACKNOWLEDGMENT

The authors acknowledge partial funding from NSF DMR-1006776 and CBET-0854979. We would also like to thank KSV Instruments (Biolin), Agilent Technologies, Malvern Instruments, and Optrel for their technical support.

■ REFERENCES

(1) Wijnhoven, J. E. G. J.; Vos, W. L. *Science* **1998**, *281*, 802–804.
(2) Tetreault, N. T.; Miguez, H.; Ozin, G. A. *Adv. Mater.* **2004**, *16*, 1471–1476.
(3) Lodahl, P.; Driel, A. F. V.; Nikolaev, I. S.; Irman, A.; Overgaag, K.; Vanmaekelbergh, D.; Vos, W. L. *Nature* **2004**, *430*, 654–657.
(4) Jiang, P. *Angew. Chem., Int. Ed.* **2004**, *43*, 5625–5628.
(5) Cassagneau, T.; Caruso, F. *Adv. Mater.* **2002**, *14*, 1629–1633.
(6) Wang, Y.; Caruso, F. *Chem. Commun.* **2004**, 1528–1529.
(7) Qian, W.; Gu, Z.; Fujishima, A.; Sato, O. *Langmuir* **2002**, *18*, 4526–4529.
(8) Martin, C. R. *Science* **1994**, *266*, 1961–1966.
(9) Yuan, Z. H.; Huang, H.; Dang, H. Y.; Cao, J. E.; Hu, B. H.; Fan, S. *Appl. Phys. Lett.* **2001**, *78*, 3127–3129.

(10) Rahman, S.; Yang, H. *Nano Lett.* **2003**, *3*, 439.
(11) Park, M.; Harrison, C.; Chaikin, P. M.; Register, R. A.; Adamson, D. H. *Science* **1997**, *276*, 1401–1404.
(12) Morey, M. S.; O'Brien, S.; Schwarz, S.; Stucky, G. D. *Chem. Mater.* **2000**, *12*, 898–911.
(13) Cheng, W.; Baudrin, E.; Dunn, B.; Zink, J. I. *J. Mater. Chem.* **2001**, *11*, 92–97.
(14) Grosso, D.; Boissiere, C.; Smarsly, B.; Brezesinski, T.; Pinna, N.; Albouy, P. A.; Amenitsch, H.; Antonietti, M.; Sanchez, C. *Nat. Mater.* **2004**, *3*, 787–792.
(15) Holland, B. T.; Blanford, C. F.; Stein, A. *Science* **1998**, *281*, 538–540.
(16) Jiang, P.; Bertone, J. F.; Colvin, V. L. *Science* **2001**, *291*, 453–457.
(17) Norell, M. A.; Makovicky, P.; Clark, J. M. *Nature* **1997**, *389*, 447–448.
(18) Velev, O, D.; Tessier, P. M.; Lenhoff, A. M.; Kaler, E. W. *Nature* **1999**, *401*, 548.
(19) Jiang, P.; Cizeron, J.; Bertone, J. F.; Colvin, V. L. *J. Am. Chem. Soc.* **1999**, *121*, 7957–7958.
(20) Zakhidov, A. A.; Baughman, R. H.; IqbaL, Z.; Cui, C.; Khayrullin, I.; Dantas, S. O.; Marti, J.; Ralchenko, V. G. *Science* **1998**, *282*, 897–901.
(21) Deutsch, M.; Vlasov, Y. A.; Norris, D. J. *Adv. Mater.* **2000**, *12*, 1176–1180.
(22) Sumida, T.; Wada, Y.; Kitamura, T.; Yanagida, S. *Chem. Commun.* **2000**, 1613–1614.
(23) Ghanem, M. A.; Bartlett, P. N.; de Groot, P.; Zhukov, A. *Electrochem. Commun.* **2004**, *6*, 447–453.
(24) Bartlett, P. N.; Birkin, P. R.; Ghanem, M. A.; Toh, C.-S. *J. Mater. Chem.* **2001**, *11*, 849–853.
(25) Cassagneau, T.; Caruso, F. *Adv. Mater.* **2002**, *14*, 1837–1841.
(26) Cassagneau, T.; Caruso, F. *Adv. Mater.* **2002**, *14*, 34–38.
(27) Wang, D.; Caruso, F. *Adv. Mater.* **2001**, *13*, 350–353.
(28) Tian, S.; Wang, J.; Jonas, U.; Knoll, W. *Chem. Mater.* **2005**, *17*, 5726–5730.
(29) Lee, J.-M.; Lee, D. G.; Kim, J. H.; Cheong, I. W. *Macromolecules* **2007**, *40*, 9529–9536.
(30) Kaiser, A. B. *Adv. Mater.* **2001**, *13*, 927–941.
(31) Leclerc, M.; Faid, K. *Adv. Mater.* **1997**, *9*, 1087–1094.
(32) Swager, T. M. *Acc. Chem. Res.* **1998**, *31*, 201–207.
(33) Ma, Y.; Zhang, J.; Zhang, G.; He, H. *J. Am. Chem. Soc.* **2004**, *126*, 7097–7101.
(34) Goto, H.; Okamoto, Y.; Yashima, E. *Macromolecules* **2002**, *35*, 4590–4601.
(35) Patil, A. O.; Heeger, A. J.; Wudl, F. *Chem. Rev.* **1988**, *88*, 183–200.
(36) Garnier, F. *Adv. Mater.* **1989**, *1*, 117–121.
(37) Geissler, M.; Xia, Y. *Adv. Mater.* **2004**, *16*, 1249–1269.
(38) Tu, H.; Heitzman, C. E.; Braun, P. V. *Langmuir* **2004**, *20*, 8313–8320.
(39) Alarcon, C. H.; Farhan, T.; Osborne, V. L.; Huck, W. T. S.; Alexander, C. *J. Mater. Chem.* **2005**, *15*, 2089–2094.
(40) Mahajan, N.; Lu, R.; Wu, S.-T.; Fang, J. *Langmuir* **2005**, *21*, 3132.
(41) Kim, P.; Lee, S. E.; Jung, H. S.; Lee, H. Y.; Kawai, T.; Suh, K. *Lab Chip* **2006**, *6*, 54–59.
(42) Del Campo, A.; Arzt, E. *Chem. Rev.* **2008**, *108*, 911–945.
(43) Jones, D. M.; Smith, J. R.; Huck, W. T. S.; Alexander, C. *Adv. Mater.* **2002**, *14*, 1130–1134.
(44) Paul, K. E.; Prentiss, M.; Whitesides, G. M. *Adv. Funct. Mater.* **2003**, *13*, 259–263.
(45) Ahn, S. J.; Kaholek, M.; Lee, W.-K.; LaMattina, B.; LaBean, T. H.; Zauscher, S. *Adv. Mater.* **2004**, *16*, 2141–2145.
(46) Kaholek, M.; Lee, W.-K.; LaMattina, B.; Caster, K. C.; Zauscher, S. *Nano Lett.* **2004**, *4*, 373–376.
(47) Werne, T. A. V.; Germack, D. S.; Hagberg, E. C.; Sheares, V. V.; Hawker, C. J.; Carter, K. R. *J. Am. Chem. Soc.* **2003**, *125*, 3831–3838.
(48) Marquez, M.; Grady, B. P. *Langmuir* **2004**, *20*, 10998–11004.
(49) Bartlett, P. N.; Birkin, P. R.; Ghanem, M. A. *Chem. Commun.* **2000**, 1671–1672.
(50) Bartlett, P. N.; Baumberg, J. J.; Birkin, P. R.; Ghanem, M. A.; Netti, M. C. *Chem. Mater.* **2002**, *14*, 2199–2208.
(51) Sumida, T.; Wada, Y.; Kitamura, T.; Yanagida, S. *Langmuir* **2002**, *18*, 3886–3894.
(52) Duan, G.; Cai, W.; Li, Y.; Li, Z.; Cao, B.; Luo, Y. *J. Phys. Chem. B* **2006**, *110*, 7184–7188.
(53) Mallon, C. T.; Jose, B.; Forster, R. J.; Keyes, T. E. *Chem. Commun.* **2010**, *46*, 106–108.
(54) Hu, J.; Abdelsalam, M.; Bartlett, P.; Cole, R.; Sugawara, Y.; Baumberg, J.; Mahajan, S.; Denuault, G. *J. Mater. Chem.* **2009**, *19*, 3855–3858.
(55) Cao, B.; Cai, W.; Sun, F.; Li, Y.; Lei, Y.; Zhang, L. *Chem. Commun.* **2004**, 1604–1605.
(56) Inaoka, S.; Roitman, D. B.; Advincula, R. C. *Chem. Mater.* **2005**, *17*, 6781–6789.
(57) Baba, A.; Onishi, K.; Knoll, W.; Advincula, R. C. *J. Phys. Chem. B* **2004**, *108*, 18949–18955.
(58) Frau, A. F.; Pernites, R. B.; Advincula, R. C. *Ind. Eng. Chem. Res.* **2010**, *49*, 9789–9797.
(59) Baba, A.; Knoll, W.; Advincula, R. *Rev, Sci. Inst.* **2006**, *77*, 064101–1−064101−6.
(60) Taranekar, P.; Baba, A.; Park, J.; Fulghum, T.; Advincula, R. *Adv. Funct. Mater.* **2006**, *16*, 2000–2007.
(61) Pernites, R.; Ponnapati, R.; Advincula, R. *Macromolecules* **2010**, *43*, 9724–9735.
(62) Taranekar, P.; Fulghum, T.; Patton, D.; Ponnapati, R.; Clyde, G.; Advincula, R. *J. Am. Chem. Soc.* **2007**, *129*, 12537–12548.
(63) Patton, D.; Taranekar, P.; Fulghum, T.; Advincula, R. C. *Macromolecules* **2008**, *41*, 6703–6713.
(64) Baba, A.; Tian, S.; Stefani, F.; Xia, C.; Wang, Z.; Advincula, R.; Johannsmann, D.; Knoll, W. *J. Electroanal. Chem.* **2004**, *562*, 95–103.
(65) Ambrose, J. F.; Nelson, R. F. *J. Electrochem. Soc.* **1968**, *115*, 1159–1164.
(66) Xia, C.; Advincula, R. C. *Chem. Mater.* **2001**, *13*, 1682–1691.
(67) Ambrose, J. F.; Carpenter, L.; Nelson, R. *J. Electrochem. Soc.* **1975**, *122*, 876–894.
(68) Sarac, S.; Ates, M.; Parlak, E.; Turcu, E. F. *J. Electrochem. Soc.* **2007**, *154*, D283–D291.
(69) Ravindranath, R.; Ajikumar, P. K.; Bahulayan, S.; Hanafiah, N. B. M.; Baba, A.; Advincula, R.; Knoll, W.; Valiyaveettil, S. *J. Phys. Chem. B* **2007**, *111*, 6336–6343.
(70) Deore, B.; Chen, Z.; Nagaoka, T. *Anal. Sci.* **1999**, *15*, 827–828.
(71) Fulghum, T.; Karim, A.; Baba, A.; Taranekar, P.; Nakai, T.; Masuda, T.; Advincula, R. *Macromolecules* **2006**, *39*, 1467–1473.
(72) MacDiarmid, A. G. *Angew. Chem., Int. Ed.* **2001**, *40*, 2581–2590.
(73) Apodaca, D. C.; Pernites, R. B.; Ponnapati, R. R.; Del Mundo, F. R.; Advincula, R. *ACS Appl. Mater. Interfaces* **2010**, DOI: 10.1021/am100805y.
(74) Tria, M. C. R.; Grande, C. D. T.; Ponnapati, R. R.; Advincula, R. C. *Biomacromolecules* **2010**, *11*, 3422–3431.
(75) Taoudi, H.; Bernède, J.; del Valle, M.; Bonnet, A.; Molinie, P.; Morsli, M.; Diaz, F.; Tregouet, Y.; Bareau, A. *J. Appl. Polym. Sci.* **2000**, *75*, 1561–1568.
(76) Abe, S.; Bernede, J.; Ugalde, L.; Tregouet, Y.; Del Valle, M. *J. Appl. Polym. Sci.* **2007**, *106*, 1568–1575.
(77) Louette, P.; Bodino, F.; Pireaux, J. J. *Surf. Sci. Spectra* **2005**, *12*, 69–73.
(78) Taoudi, H.; Bernede, J.; Bonnet, A.; Morsli, M.; Godoy, A. *Thin Solid Films* **1997**, *304*, 48–55.
(79) Sohn, Y.; Pradhan, D.; Radi, A.; Leung, K. T. *Langmuir* **2009**, *25*, 9557–9563.
(80) Liu, Y.; Klep, V.; Luzinov, I. *J. Am. Chem. Soc.* **2006**, *128*, 8106–8107.
(81) Ishida, T.; Hara, M.; Kojima, I.; Tsuneda, S.; Nishida, N.; Sasabe, H.; Knoll, W. *Langmuir* **1998**, *14*, 2092–2096.

(82) Zubragel, C.; Deuper, C.; Schneider, F.; Neumann, M.; Grunze, M.; Schertel, A.; Woll, K. *Chem. Phys. Lett.* **1995**, *238*, 308–312.
(83) Castner, D. G.; Hinds, K.; Grainger, D. W. *Langmuir* **1996**, *12*, 5083–5086.
(84) Felipe, M. J. L.; Ponnapati, R. R.; Pernites, R. B.; Dutta, P.; Advincula, R. C. *ACS Appl. Mater. Interfaces* **2010**, *2*, 3401–3405.